

LETTER TO THE EDITOR

# The young exoplanetary system TOI-4562: Confirming the presence of a third body in the system

V. Fermiano<sup>1</sup>, R. K. Saito<sup>1</sup>, V. D. Ivanov<sup>2</sup>, C. Caceres<sup>3</sup>, L. A. Almeida<sup>4</sup>, J. Aires<sup>5</sup>, J. C. Beamin<sup>6</sup>, D. Minniti<sup>3,7</sup>, T. Ferreira<sup>8</sup>, L. Andrade<sup>9</sup>, B. W. Borges<sup>10</sup>, L. de Almeida<sup>9</sup>, F. Jablonski<sup>11</sup>, and W. Schindwein<sup>11</sup>

<sup>1</sup> Departamento de Física, Universidade Federal de Santa Catarina, Trindade 88040-900, Florianópolis, Brazil

<sup>2</sup> European Southern Observatory, Karl Schwarzschildstr 2, D-85748, Garching bei München, Germany

<sup>3</sup> Instituto de Astrofísica, Dep. de Ciencias Físicas, Facultad de Ciencias Exactas, Universidad Andres Bello, Av. Fernández Concha 700, Santiago, Chile

<sup>4</sup> Escola de Ciências e Tecnologia, Universidade Federal do Rio Grande do Norte, Campus Universitário, Natal, RN, 59072-970, Brazil

<sup>5</sup> Departamento de Física, Universidade Federal do Rio Grande do Norte, 59072-970, Natal-RN, Brazil

<sup>6</sup> Fundación Chilena de Astronomía, El Vergel 2252, Santiago, Chile

<sup>7</sup> Vatican Observatory, Specola Vaticana, V-00120, Vatican City, Vatican City State

<sup>8</sup> Department of Astronomy, Yale University, 219 Prospect Street, New Haven, CT 06511, USA

<sup>9</sup> Laboratório Nacional de Astrofísica, Rua Estados Unidos 154, 37504-364, Itajubá-MG, Brazil

<sup>10</sup> Coordenadoria Especial de Física, Química e Matemática, Universidade Federal de Santa Catarina, Jardim das Avenidas 88906-072, Araranguá, Brazil

<sup>11</sup> Instituto Nacional de Pesquisas Espaciais, Avenida dos Astronautas, 1758, São José dos Campos-SP, Brazil

Received September 15, 1996; accepted March 16, 2999

## ABSTRACT

**Context.** Young planetary systems represent an opportunity to investigate the early stages of (exo)planetary formation because the gravitational interactions have not yet significantly changed the initial configuration of the system.

**Aims.** TOI-4562 b is a highly eccentric temperate Jupiter analogue orbiting a young F7V-type star of < 700 Myr in age with an orbital period of  $P_{orb} \sim 225$  days and an eccentricity of  $e = 0.76$ , and is one of the largest known exoplanets to have formed in situ.

**Methods.** We observed a new transit of TOI-4562 b using the 0.6-m Zeiss telescope at the Pico dos Dias Observatory (OPD/LNA) in Minas Gerais, Brazil, and combine our data with Transiting Exoplanet Survey Satellite (TESS) and archive data, with the aim being to improve the ephemerides of this interesting system.

**Results.** The  $O - C$  diagram for the new ephemeris is consistent with the presence of a giant planet in an outer orbit around TOI-4562. TOI-4562 c is a planet with a mass of  $M = 5.77 M_{Jup}$ , an orbital period of  $P_{orb} = 3990$  days, and a semi-major axis of  $a = 5.219$  AU.

**Conclusions.** We report the discovery of TOI-4562 c, the exoplanet with the longest orbital period discovered to date via the transit timing variation (TTV) method. The TOI-4562 system is in the process of violent evolution with intense dynamical changes — judging by its young age and high eccentricity — and is therefore a prime target for studies of formation and evolution of planetary systems.

**Key words.** Planets and satellites: formation — Planets and satellites: dynamical evolution and stability — Stars: activity

## 1. Introduction

Young stellar systems provide a unique window onto the early stages of planetary evolution, which are marked by dynamic processes and rapid changes. These systems undergo significant transformations as they interact and evolve, and studying young systems offers valuable insights into the formation and evolution of planets. By examining young stellar systems, we gain a fundamental understanding of the mechanisms that drive planetary formation and the initial conditions that shape the diversity of planetary architectures observed in mature systems.

TOI-4562 b (=TIC 349576261) is a highly eccentric temperate Jupiter analogue discovered by Heitzmann et al. (2023, hereafter HEI23). The planet orbits a young F7V-type star of <700 Myr in age with an orbital period of  $P_{orb} = 225.11781^{+0.00025}_{-0.00022}$  days and an eccentricity of  $e = 0.76 \pm 0.02$

(HEI23). Combining transits from the Transiting Exoplanet Survey Satellite (TESS) satellite with a transit from a ground-based telescope, and spectroscopic data, HEI23 measured the planet's radius and mass as  $R_p = 1.118^{+0.013}_{-0.014} R_{Jup}$  and  $M_p = 2.30^{+0.48}_{-0.47} M_{Jup}$ . The HEI23 ephemeris for TOI-4562 b results in an observed-minus-calculated variation (' $O - C$ ' or 'TTV', short for transit timing variation) at the  $\sim 3$ –15 minute level for all five transits used in their analysis, suggesting the presence of a third body.

We observed a transit of TOI-4562 b at the Pico dos Dias Observatory (OPD/LNA) in Brazil on November 9 2023, which, much to our surprise, occurred  $\sim 2$  hours earlier than expected according to the HEI23 ephemeris ( $O - C = 116$  min.). By combining this new event time with the existing data from TESS and ground-based observations, we were able to provide a new ephemeris for TOI-4562 b whose TTV diagram is consistent with the presence of a giant gas planet in an outer or-

Send offprint requests to: vitorfreitasfermiano@outlook.com

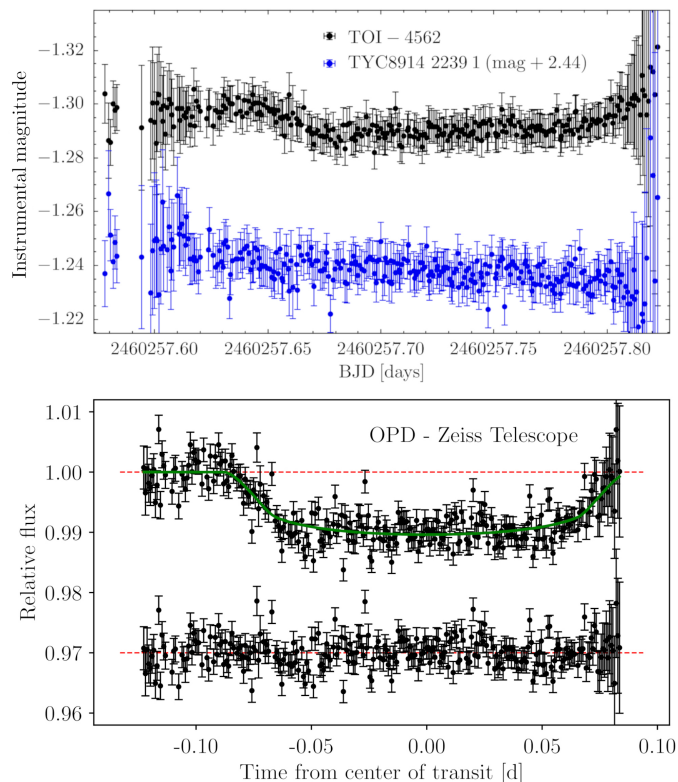


**Fig. 1.** Transit of TOI-4562 b observed at the OPD/LNA on the night of UT 2023 Nov 9. Top panel: Raw data of TOI-4562 b and the standard star TYC 8914-2239-1 collected at the OPD/LNA. The y-axis is the instrumental magnitude with the data of TYC 8914-2239-1 displaced by +2.44 mag for visualisation purposes. Bottom panel: Normalised transit of TOI-4562 b (black data-points) and the modelled transit signal (green solid line). Midtransit occurred at  $T_{mid}(BJD) = 2,460,257.73350$ , resulting in an  $O-C$  of  $\sim 2$  hours in relation to the HEI23 ephemeris. The residuals after the fitting of the transit model are also shown. Fig. A.1 in the Appendix complements the fit for the OPD transit, showing the fits for the five TESS transits.

bit around TOI-4562. Here we report the discovery of TOI-4562 c, a Jupiter-size planet of  $M_p = 5.77 M_{Jup}$  with an orbit of  $P_{orb} = 3990$  days, and semi-major axis  $a \sim 5.22$  AU. TOI-4562 c is the longest-period TTV-discovered exoplanet to date<sup>1</sup>.

## 2. Ground-based observations of TOI-4562

Ground-based observations of TOI-4562 were carried out with the 0.6-m f/12.5 Zeiss telescope at the Pico dos Dias Observatory on UT November 9 2023. OPD/LNA is located in the Brazilian state of Minas Gerais ( $22^\circ 32' 04''$  S,  $45^\circ 34' 57''$  W) at an altitude of 1,864 m above sea level. TOI-4562 is at coordinates RA, Dec (J2000) = 07:28:02.41,  $-63:31:04$ , thus allowing good coverage starting at 2023 Nov 9 UT 01:51:33, with an airmass of 2.45 (corresponding to an altitude of  $23^\circ$ ), reaching a minimum airmass of 1.32 at UT  $\sim 07:20$ . The observations were concluded at 2023 Nov 9 UT 07:46:10, with an airmass of 1.35 (altitude  $48^\circ$ ). For TOI-4562 b observations, the telescope was equipped with an Andor iXon EMCCD camera, with a field of view (FoV) of approximately  $6 \times 6$  arcmin.

The observations of TOI-4562 b were conducted with the R filter ( $\lambda_C \sim 6450$  Å), an exposure time of 60 seconds and read-

<sup>1</sup> According to the NASA Exoplanet Archive on the time of writing (<https://exoplanetarchive.ipac.caltech.edu/>)

out time of 2.3 seconds, thus allowing a cadence of  $\sim 1$  minute (62.3 sec). This coverage should allow observation of the first half of the TOI-4562 b transit (cycle #8, according to HEI23 ephemeris), which would have its midtransit near the twilight time in the OPD/LNA. The observations were taken under good atmospheric conditions and the photometric data were reduced using standard IRAF tasks to produce the TOI-4562 b light curve. Eight field stars were used for the differential photometry, with TYC 8914-2239-1 ( $V = 11.43$  mag and  $r = 11.08$  mag; Munari et al. 2014) as the main reference. The unreduced data of TOI-4562 b and TYC 8914-2239-1 collected at the OPD/LNA are presented in the top panel of Fig. 1, while the normalised transit of TOI-4562 b is shown in its bottom panel. The data for the latter are available in Table A.1 in the Appendix.

Our updated ephemeris (discussed in Section 4) suggests that another transit of TOI-4562 b — cycle #9 according to the HEI23 ephemeris — was expected to occur on 21 June 2024, with the midtransit at 08:06:51 UT. Although the transit the OPD/LNA was able to partially observe the transit, the extremely low elevation of  $\lesssim 10$  deg prevented data collection.

## 3. Data archive searches

TOI-4562 lies in the TESS southern continuous viewing zone and was photometrically monitored with almost no interruptions during years 1 and 3 of operations. The star was observed at a cadence of 30 min during Sectors 1-8 (from July 25 2018 to February 28 2019) and Sectors 10-13 (March 26 2019 to July 18 2019), at a cadence of 2 min during Sectors 27–39 (from July 4 2020 to June 24 2021), and at a cadence of 20 sec in sector 63 (March 10 2023 to April 6 2023). The first transit signature of TOI-4562 b was detected by the TESS Science Processing Operations Center (Jenkins et al. 2016), and the object was designated as a TESS Object of Interest (TOI) in 2021.

We retrieved all available TESS data for TOI-4562 using `lightkurve` (Lightkurve Collaboration et al. 2018), which were processed with the SPOC pipeline (Jenkins et al. 2016, 2020). A total of five transits of TOI-4562 b were found in TESS light curves, including a new event that occurred on March 29 2023 (cycle #7). The four previous events were used by HEI23 in their analysis (cycles #0, #1, #3 and #4). The timing of a TOI-4562 b transit observed on January 3 2022 at the LCOGT's South African Astronomical Observatory (SAAO) node using two 1 m telescopes (details in HEI23) was also included in our analysis.

## 4. Data analysis

The aim of our analysis is to understand the variation of the  $O-C$  detected in the TOI-4562 b transits, which could indicate the presence of a third body in the system. We first performed a transiting exoplanet light-curve fitting on the Zeiss and the five TESS light curves simultaneously. We modelled the transit signal using the `batman` package (Kreidberg 2015) together with a Markov Chain Monte Carlo (MCMC) method, implemented through the `emcee` package Foreman-Mackey et al. (2013). We considered as free parameters the planet-to-star radius  $R_{p,b}/R_\star$  for the Zeiss and TESS light curves  $k_V$  and  $k_{TESS}$ , the semi-major axis normalised to the stellar radius  $a_b/R_\star$ , the inclination angle  $i$ , and the transit times  $t_c$  for each epoch individually. We obtained all the other parameters (with their uncertainties) from HEI23, which were kept fixed during the fitting. This includes two quadratic limb-darkening coefficients  $u_1$  and  $u_2$  in the V-filter that were interpolated from the Claret (2000) tables.

**Table 1.** Midtransit instances for TOI-4562 b.

Cycle	Observed BJD [days]	Observatory	$(O - C)_{\text{HEI23}}$ [min]	Calculated BJD [days]	TTV [min]
0	2,458,456.87916 <sup>+0.00112</sup> <sub>-0.00099</sub>	TESS	+10.7712	2,458,456.900401	-30.7440
1	2,458,681.98020 <sup>+0.00092</sup> <sub>-0.00088</sub>	TESS	-13.3776	2,458,682.006969	-38.4624
3	2,459,132.21623 <sup>+0.00110</sup> <sub>-0.00111</sub>	TESS	-12.7872	2,459,132.220105	-5.0112
4	2,459,357.34510 <sup>+0.00096</sup> <sub>-0.00095</sub>	TESS	+3.1392	2,459,357.326673	+27.3456
5	2,459,582.46321 <sup>+0.00142</sup> <sub>-0.00142</sub>	LCOGT*	+3.5712	2,459,582.433241	+44.2080
7	2,460,032.64015 <sup>+0.00113</sup> <sub>-0.00111</sub>	TESS	-80.9280	2,460,032.646377	-7.4304
8	2,460,257.73350 <sup>+0.00369</sup> <sub>-0.00385</sub>	OPD/LNA	-116.1504	2,460,257.752945	-26.2224

**Notes.** The cycles are numbered according to  $T_0(\text{BJD}) = 2458456$  days. The second column shows the observed midtransits for TOI-4562 b for the seven cycles used in our analysis. For the LCOGT observations, the midtransit is from HEI23. The remaining midtransits are calculated using a multiple-transit simultaneous-fit procedure (see Section 4). Column four presents the  $O - C$  according to the HEI23 ephemeris, while columns five and six present the calculated midtransit and the respective TTVs with respect to the ephemeris obtained in this work.

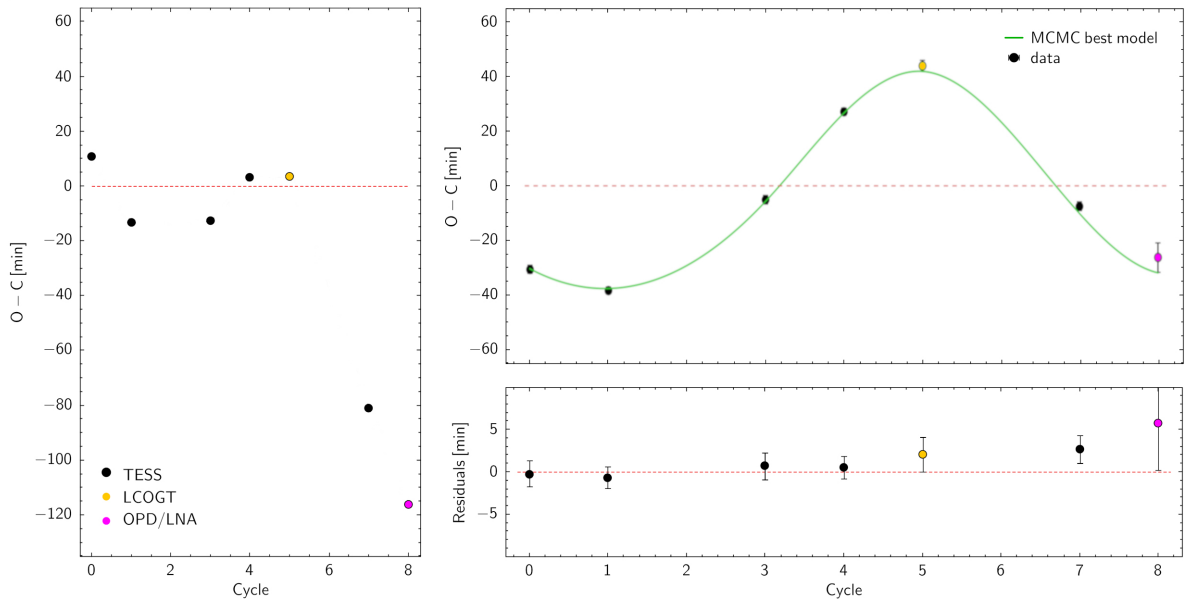


**Fig. 2.**  $O - C$  diagrams of the TOI-4562 b transit. Left panel:  $O - C$  diagram for all seven events according to the HEI23 ephemeris. In addition to the large  $O - C$  value for cycle #8 observed from OPD/LNA, the  $O - C$  for cycle #7 observed by TESS is also notable. Top right panel:  $O - C$  diagram of the TOI-4562 b transits, according to the ephemeris described in Equation 1. The observed midtransit times are shown as filled circles, while the model is shown as a green curve. Bottom right panel: Residuals from the fitting in the top right panel, with the respective error bars. The colour coding of the data points denotes the observatory and is the same in all panels: black for TESS, yellow for LCOGT, and magenta for OPD/LNA.

In addition, we included in the fit a second-order polynomial to account for the normalisation of the light curves. For the MCMC fit, we used 50,000 steps and 64 walkers, and we assumed uniform priors for all the free parameters. The parameters are summarised in Tables 1 and 2 (transit times and remaining parameters, respectively), and show good agreement with those presented in HEI23. We find that all the parameters in the fit are in agreement with those presented in HEI23.

Our next step consisted of determining the orbital period of the system and performing a polynomial fit to obtain the delays and advances in the orbital cycles of the exoplanet and thus build the  $O - C$  diagram. Using the midtransit timing for all seven events (see Table 1), a new ephemeris for TOI-4562 b was obtained, as follows:

$$T_{\text{mid}}(\text{BJD}) = 2459476.90051^{+0.00053}_{-0.00057} + 225.10640^{+0.00015}_{-0.00015} \times E. \quad (1)$$

A longer baseline produced a slightly different ephemeris with respect to that obtained by HEI23. In particular, we note that the orbital period is approximately 16 min ( $= 0.00114$  days) shorter than the previous HEI23 value, thus producing a distinct  $O - C$  diagram, as shown in Fig. 2. When fitting the transit-time measurements using a linear ephemeris, we note a possible periodic signal with a semi-amplitude of approximately 40 min. This signal could indicate the presence of an additional third body gravitationally interacting with the system.

We searched for the parameters of this possible third object by modelling the observed transit-times with the TTVFast code

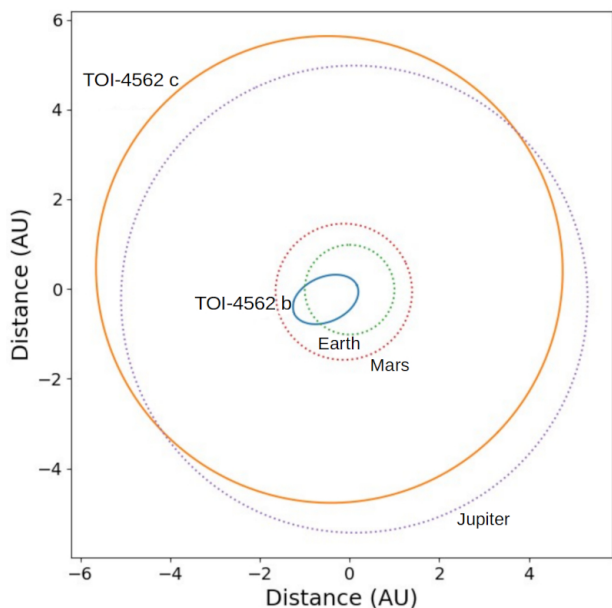


**Fig. 3.** Schematic diagram showing the orbits of TOI-4562 b and TOI-4562 c compared with planets of the Solar System. TOI-4562 c is a giant planet with 5.73 Jupiter masses in an orbit with a semi-major axis of 5.22 AU and an orbital period of 3990 days.

(Deck et al. 2014), which is a modified n-body simulation code that uses a WH integrator (Wisdom & Holman 1991) with a Keplerian orbit interpolator to calculate transit times and TTVs in transiting planetary systems (Deck et al. 2014; Agol, Hernandez, & Langford 2021). The code requires the parameters of both bodies, the mass of the star, and the time and the time-step for the integration. We took the TOI-4562 mass and TOI-4562 b parameters given by HEI23, and integrated from BJD 2458254 to BJD 2460258 with a time-step of 0.01 days. The parameters of the third body and those of TOI-4562 b that do not appear in HEI23 were taken as free parameters and were determined using a MCMC procedure from the emcee package. At each step of the MCMC, we used the generated values to compute the transit times of the observed planet and compared them with the observed times through a  $\chi^2$  goodness-of-fit estimation, that is,

$$\chi^2 = \sum_i^n \left( \frac{O_i - C_i}{\sigma_i} \right)^2, \quad (2)$$

where  $O_i$  are the observed times,  $C_i$  are the corresponding computed times, and  $\sigma_i$  are the errors in the observations.

As free parameters, we use the mass of the third body ( $M_c$ ), the orbital period ( $P_c$ ), the eccentricity ( $e_c$ ), the longitude of the ascending node ( $\Omega_c$ ), the periastron argument ( $\omega_c$ ), and the mean anomaly ( $\mathcal{M}_c$ ), together with the longitude of the ascending node ( $\Omega_b$ ) and the mean anomaly ( $\mathcal{M}_b$ ) of the transiting body. We manually searched for the best initial values of the free parameters to start the MCMC. The priors were distributed normally around the initial values. We used 16 walkers (twice the number of free parameters) and 5,000 steps, discarding the first 100 steps as burn-in. Table 2 lists the median values and the  $1\sigma$  confidence interval ( $\pm 34\%$ ) obtained from the a posteriori distributions. The corner plot with the posterior distributions of the parameters is shown in Fig. A.2 in the Appendix.

Figure 2 shows the best solution for the midtransits together with the observed transit times. The next five upcoming events of TOI-4562 b are presented in the Appendix (see Table A.2 and

**Table 2.** Parameters of TOI-4562 b and TOI-4562 c

Parameter	Description	Value
<b>TOI-4562 b</b>		
$k_{\text{OPD/LNA}}$	Planet-to-star radius	$0.0960^{+0.0071}_{-0.0075}$
$k_{\text{TESS}}$	Planet-to-star radius	$0.09485^{+0.0015}_{-0.0015}$
$a/R_s$	Normalised semi-major axis	$150.3^{+12.4}_{-9.8}$
$i$	Orbit inclination [deg]	$+89.15^{+0.21}_{-0.17}$
$u_1$	Limb-darkening coefficient	0.41
$u_2$	Limb-darkening coefficient	0.29
$T_0$	Linear ephemeris [BJD]	$2459476.90040^{+0.00051}_{-0.00059}$
$P_{\text{orb}}$	Orbital period [days]	$225.10640^{+0.00015}_{-0.00015}$
$\Omega_b$	Longitude of the ascending node [deg]	$24^{+17}_{-16}$
$\mathcal{M}_b$	Mean anomaly [deg]	$38.297 \pm 0.004$
<b>TOI-4562 c</b>		
$M_P$	Mass Planet [ $M_{\text{jup}}$ ]	$5.77^{+0.37}_{-0.56}$
$P_{\text{orb}}$	Orbital period [days]	$3990^{+201}_{-192}$
$e$	Eccentricity	$0.122^{+0.027}_{-0.026}$
$a$	Semimajor axis [AU]	$5.219 \pm 0.002$
$\omega$	Argument of periastron [deg]	$3^{+20}_{-21}$
$i$	Orbit inclination [deg]	$90.00^{+0.17}_{-0.19}$
$\Omega_c$	Longitude of the ascending node [deg]	$-57^{+23}_{-24}$
$\mathcal{M}_c$	Mean anomaly [deg]	$194^{+24}_{-23}$

**Notes.** Orbital parameters of TOI-4562 b and TOI-4562 c derived from our analysis. A corner plot for the posterior distribution of our free parameters is presented in Fig. A.2 of the Appendix.

Fig. A.3). Figure 3 shows the schematic diagram of the TOI-4562 system compared with planets of the Solar System.

## 5. Discussion

Young planetary systems such as TOI-4562 represent an opportunity to observe the early stages of planetary formation. In the first million years of the life of these systems, gravitational interactions have not yet significantly changed their initial configuration (e.g. Martioli et al. 2021). Figure 3 shows a schematic diagram of the TOI-4562 system compared with planets of the Solar System. TOI-4562 c is the planet with the largest period found so far using the TTV technique. The large TTV amplitude may be an indication of planetary migration, although the ratio between orbits is very high and there is no indication of resonance between the planets ( $P_c/P_b \sim 17.7$ ). In addition, the orbit of TOI-4562 b is one of the most eccentric among exoplanets with indications of in situ formation (e.g. Chabrier et al. 2014).

The TTV method is susceptible to dynamic degeneracies between planet eccentricity and planet mass, and perturbations

caused by non-transiting planets can be misattributed to transiting planets (Weiss 2016). This degeneracy can be broken with additional information such as radial-velocity measurements, as in the analysis of TOI-4562 b by HEI23; or the assumption of stability of the planetary system (Fabrycky et al. 2012; Lithwick, Xie, & Wu 2012; Weiss et al. 2017), which is unlikely here given the youth of TOI-4562. In our TTV analysis, we kept the mass of TOI-4562 b as a prior and fixed parameter with the value (and uncertainties) as reported by HEI23 to minimise this degeneracy effect, thus decreasing the probability of solutions with similar residuals for different configurations of planet mass and eccentricity for TOI-4562 c.

Other possible interpretations of the TTV signal may include the consideration that TOI-4562 is made up of only the star and the transiting planet. Firstly, there is the possibility that TTV is caused by stellar activity. The most plausible explanation entailing dynamical interaction with the star, causing the TTV signal, is the Applegate effect (Applegate 1992) applied to exoplanets, as described in Watson & Marsh (2010). According to this effect, the star undergoes a magnetic cycle that alters the gravitational pull of its rotational bulge on the planet, causing slight variations in its orbital period. To produce the observed TTV signal, the magnetic cycle would need to have a period of  $\sim 1995$  days (the initial fit for the TTV signal). For magnetic dynamos typical of solar-type stars like Kepler-19, Watson & Marsh (2010) calculate TTV variations of less than 1 second over timescales of several years; too small to explain our data. In addition to this dynamical interaction, activity could cause an apparent TTV due to the planet's transit over starspots, and the rotation of the apsidal line of the planetary orbit.

Despite the high inclination of the orbit of TOI-4562 c, we were unable to find any signal of its transit in the available TESS data. This absence is not surprising given that the current TESS baseline of  $\sim 6$  years is shorter than the planet's orbital period of almost 11 years. Moreover, TESS does not provide continuous coverage of the TOI-4562 field. Even for planet TOI-4562 b, which has a shorter period, only half of the transits have been observed by TESS since the first detection. In addition, some of the orbital parameters that should predict the transits of planet TOI-4562 c still have high uncertainties due to the small number of transits observed for planet TOI-4562 b, from which we obtained the TTV curve. This result highlights the challenges in observing long-period exoplanets with current transit-based survey missions. Future monitoring is necessary to refine the orbital parameters for both planets in order to confirm the presence of transits for TOI-4562 c.

## 6. Conclusions

We observed a new transit of TOI-4562 b using the 0.6-m Zeiss telescope at the Pico dos Dias Observatory in Minas Gerais, Brazil, in order to improve the ephemeris of this interesting system. The  $O - C$  diagram considering our observation, together with all the other transits observed with TESS and the LCOGT transit available in the literature, allowed us to detect the presence of a giant planet in an outer orbit around TOI-4562. We report the discovery of TOI-4562 c, a planet with a mass of  $M = 5.77 M_{Jup}$  with an orbital period of  $P_{orb} = 3990$  days, and a semi-major axis of  $a = 5.219$  AU. To the best of our knowledge, this is the exoplanet with the largest orbital period discovered using the TTV method known to date. There is also no sign of resonance between the orbits of the planets, with the TOI-4562 b orbit being one of the most eccentric known. The TOI-4562 system is in the process of violent evolution and intense dynamical

changes — judging by its young age and the high eccentricity of the TOI-4562 b planet — and is therefore a prime target for studies of the formation and evolution of planetary systems.

*Acknowledgements.* This work uses observations made at the Observatorio do Pico dos Dias/LNA (Brazil). Funding for the TESS mission is provided by NASA's Science Mission Directorate. V.F. acknowledges support from CNPq/Brazil and Universidade Federal de Santa Catarina (UFSC) through programs BIP/UFSC and PIBIC/UFSC. R.K.S. acknowledges support from CNPq/Brazil through project 308298/2022-5. R.K.S., L.A.A. and F.J. acknowledge support from CNPq/Brazil through project 421034/2023-8. C.C. acknowledges support by ANID BASAL project FB210003. D.M. acknowledges support by Fondecyt Project No. 1220724, and by the Center for Astrophysics and Associated Technologies ANID BASAL projects ACE210002 and FB210003.

## References

- Agol E., Hernandez D. M., Langford Z., 2021, *MNRAS*, 507, 1582. doi:10.1093/mnras/stab2044
- Applegate J. H., 1992, *ApJ*, 385, 621. doi:10.1086/170967
- Chabrier G., Johansen A., Janson M., Rafikov R., 2014, *prpl.conf*, 619. doi:10.2458/azu\_uapress\_9780816531240-ch027
- Claret A., 2000, *A&A*, 363, 1081
- Deck K. M., Agol E., Holman M. J., Nesvorný D., 2014, *ApJ*, 787, 132. doi:10.1088/0004-637X/787/2/132
- Foreman-Mackey D., Hogg D. W., Lang D., Goodman J., 2013, *PASP*, 125, 306. doi:10.1086/670067
- Heitzmann A., Zhou G., Quinn S. N., Huang C. X., Dong J., Bouma L. G., Dawson R. I., et al., 2023, *AJ*, 165, 121. doi:10.3847/1538-3881/acb5a2
- Jenkins J. M., Twicken J. D., McCauliff S., Campbell J., Sanderfer D., Lung D., Mansouri-Samani M., et al., 2016, *SPIE*, 9913, 99133E. doi:10.1117/12.8
- Jenkins J. M., Twicken J. D., Tenenbaum P., Ting E. B., Caldwell D. A., Smith J., Rose M., et al., 2020, *DPS*
- Kasting J. F., Whitmire D. P., Reynolds R. T., 1993, *Icar*, 101, 108. doi:10.1006/icar.1993.1010
- Kreidberg L., 2015, *PASP*, 127, 1161. doi:10.1086/683602
- Kopparapu R. K., Ramirez R., Kasting J. F., Eymet V., Robinson T. D., Mahadevan S., Terrien R. C., et al., 2013, *ApJ*, 765, 131. doi:10.1088/0004-637X/765/2/131
- Lightkurve Collaboration, Cardoso J. V. de M., Hedges C., Gully-Santiago M., Saunders N., Cody A. M., Barclay T., et al., 2018, *ascl.soft.1812.013*
- Martioli E., Hébrard G., Correia A. C. M., Laskar J., Lecavelier des Etangs A., 2021, *A&A*, 649, A177. doi:10.1051/0004-6361/202040235
- Munari U., Henden A., Frigo A., Zwitter T., Bienaymé O., Bland-Hawthorn J., Boeche C., et al., 2014, *AJ*, 148, 81. doi:10.1088/0004-6256/148/5/81
- Watson C. A., Marsh T. R., 2010, *MNRAS*, 405, 2037. doi:10.1111/j.1365-2966.2010.16602.x
- Wisdom J., Holman M., 1991, *AJ*, 102, 1528. doi:10.1086/115978
- Fabrycky D. C., Ford E. B., Steffen J. H., Rowe J. F., Carter J. A., Moorhead A. V., Batalha N. M., et al., 2012, *ApJ*, 750, 114. doi:10.1088/0004-637X/750/2/114
- Lithwick Y., Xie J., Wu Y., 2012, *ApJ*, 761, 122. doi:10.1088/0004-637X/761/2/122
- Weiss L. M., 2016, *PhDT*
- Weiss L. M., Deck K. M., Sinukoff E., Petigura E. A., Agol E., Lee E. J., Becker J. C., et al., 2017, *AJ*, 153, 265. doi:10.3847/1538-3881/aa6c29



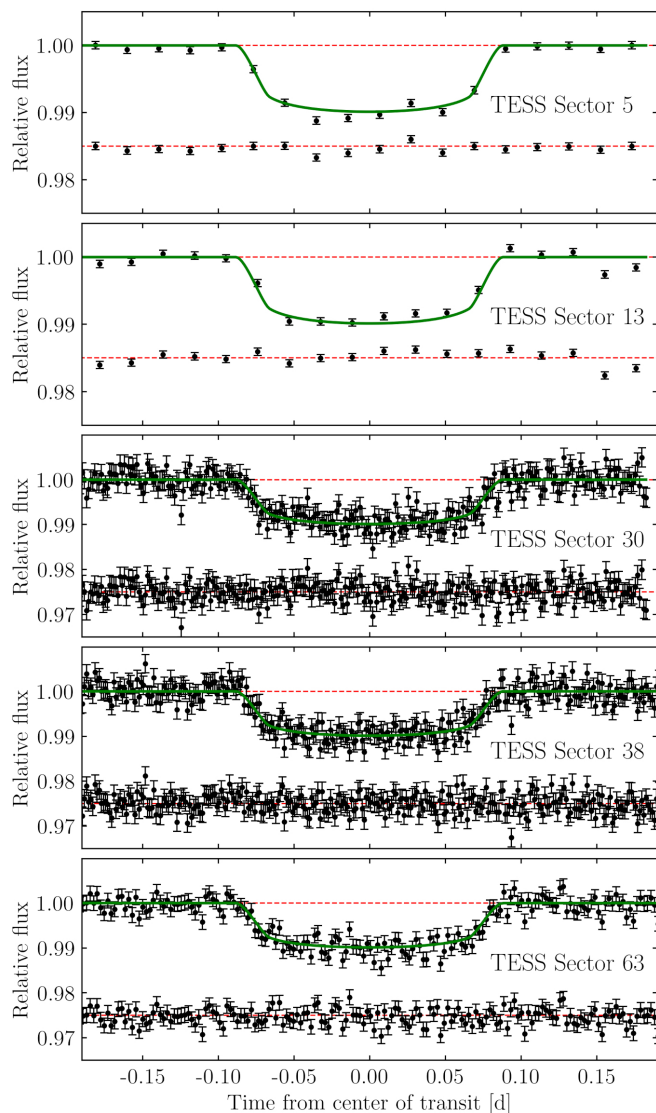


**Fig. A.1.** TESS light curves and respective simultaneous multi-transit fit for five transits of TOI-4562 b. The panels correspond to cycles #0, #1, #3 and #4 and #7, from top to bottom. Cycle #7 is the as-yet-unpublished event occurred on March 29, 2023. Phase 0.00 in the light curves corresponds to the instants of midtransit listed in the 1st column of Table 1.

## Appendix A: Complementary material

### Appendix A.1: Simultaneous multi-transit fit of the TESS observations

As described in Section 2 and 3, we used a total of 7 transits of TOI-4562 b in our analysis. With the exception of the transit obtained at the LCOGT and described by HEI23, for all other TESS transits we calculated the transit midpoints independently, by performing a simultaneous multi-transit fit. Fig. A.1 complements the fit shown in Fig. 1 for the OPD transit, showing the fits for the 5 TESS transits, including the as-yet-unpublished event occurred on March 29, 2023 (Cycle #7).

### Appendix A.2: Posterior distribution of free parameters

In Section 4 we describe the process to obtain the orbital parameters of TOI-4562 c, by modelling the posterior probability using the Markov Chain Monte Carlo (MCMC) method. Fig. A.2

presents the posterior distribution of our free parameters: the third-body mass ( $M_c$ ), the orbital period ( $P_c$ ), the eccentricity ( $e_c$ ), the longitude of the ascending node ( $\Omega_c$ ), the periastron argument ( $\omega_c$ ), the mean anomaly ( $M_c$ ), the transiting body longitude of the ascending node ( $\Omega_b$ ) and mean anomaly ( $M_b$ ).

### Appendix A.3: Next events for TOI-4562 b

Due to the uniqueness of TOI-4562 system, transit times for upcoming events of TOI-4562 b are presented in HEI23. This importance is greater now, with the discovery of another exoplanet in the system. The ephemeris and TTVs calculated in this work significantly changes the instants of the next transits, which is why the predicted timing for the next 5 transits of TOI-4562 b are presented in Table A.2 and Fig. A.3. As mentioned in Section 4, we could not find any sign related to the transit of the TOI-4562 c in the TESS data, but given its long period of more than a decade and the large orbit, this detection is unlikely.

**Table A.1.** Normalised light-curve of the TOI-4562 b transit observed at the OPD/LNA on 2023 Nov 9. Time corresponds to BJD–2460257.

Time [days]	Relative Flux	Time [days]	Relative Flux	Time [days]	Relative Flux	Time [days]	Relative Flux
0.610618	1.0008±0.0036	0.666149	0.9997±0.0019	0.720236	0.9881±0.0019	0.769274	0.9908±0.0018
0.611340	0.9965±0.0037	0.667591	0.9919±0.0019	0.720957	0.9933±0.0019	0.769995	0.9896±0.0018
0.612061	1.0005±0.0036	0.668312	0.9926±0.0019	0.721678	0.9916±0.0019	0.770716	0.9908±0.0018
0.612782	0.9981±0.0032	0.669033	0.9911±0.0019	0.722399	0.9923±0.0019	0.771437	0.9894±0.0018
0.613503	0.9975±0.0030	0.669754	0.9903±0.0019	0.723121	0.9916±0.0019	0.772159	0.9889±0.0019
0.614224	0.9994±0.0028	0.670475	0.9869±0.0019	0.723842	0.9916±0.0018	0.772880	0.9877±0.0018
0.614945	1.0004±0.0026	0.671197	0.9909±0.0019	0.724563	0.9918±0.0018	0.774322	0.9889±0.0018
0.615666	0.9949±0.0025	0.671918	0.9918±0.0019	0.725284	0.9887±0.0018	0.775043	0.9893±0.0018
0.616388	0.9978±0.0024	0.673360	0.9899±0.0019	0.726005	0.9906±0.0018	0.775764	0.9896±0.0018
0.617109	1.0071±0.0024	0.674081	0.9899±0.0019	0.726726	0.9892±0.0019	0.776485	0.9890±0.0018
0.617830	0.9945±0.0023	0.674802	0.9894±0.0019	0.727447	0.9889±0.0019	0.777206	0.9915±0.0018
0.618551	1.0029±0.0022	0.675523	0.9932±0.0019	0.728168	0.9892±0.0018	0.777928	0.9960±0.0019
0.619273	1.0010±0.0022	0.676244	0.9898±0.0019	0.728890	0.9920±0.0018	0.778649	0.9923±0.0018
0.619994	0.9995±0.0022	0.676966	0.9916±0.0018	0.729611	0.9868±0.0018	0.779370	0.9860±0.0018
0.622878	0.9968±0.0021	0.677687	0.9884±0.0019	0.730332	0.9883±0.0018	0.780091	0.9873±0.0018
0.623599	1.0003±0.0021	0.679129	0.9920±0.0019	0.731053	0.9894±0.0019	0.780812	0.9905±0.0018
0.624320	1.0006±0.0022	0.679850	0.9872±0.0019	0.731775	0.9896±0.0018	0.781533	0.9888±0.0018
0.625763	0.9944±0.0021	0.680571	0.9859±0.0019	0.732496	0.9919±0.0019	0.782254	0.9910±0.0018
0.627205	0.9996±0.0021	0.681292	0.9894±0.0019	0.733216	0.9904±0.0019	0.782975	0.9929±0.0018
0.627926	0.9989±0.0021	0.682014	0.9880±0.0019	0.733938	0.9905±0.0019	0.783696	0.9889±0.0019
0.628647	0.9972±0.0021	0.683456	0.9932±0.0019	0.734659	0.9879±0.0019	0.784417	0.9891±0.0018
0.629368	0.9990±0.0021	0.684177	0.9853±0.0019	0.735380	0.9899±0.0019	0.785138	0.9876±0.0018
0.630089	1.0011±0.0021	0.684898	0.9931±0.0019	0.736101	0.9905±0.0019	0.785860	0.9953±0.0018
0.630811	1.0045±0.0021	0.686341	0.9940±0.0019	0.736823	0.9889±0.0019	0.786581	0.9955±0.0018
0.631532	1.0001±0.0021	0.687062	0.9885±0.0019	0.737544	0.9919±0.0019	0.787302	0.9889±0.0018
0.632253	1.0032±0.0020	0.687783	0.9888±0.0019	0.738265	0.9918±0.0018	0.788023	0.9865±0.0019
0.632974	1.0020±0.0020	0.688504	0.9877±0.0019	0.738986	0.9881±0.0019	0.788744	0.9900±0.0018
0.633696	1.0017±0.0020	0.689225	0.9902±0.0019	0.739707	0.9892±0.0019	0.789466	0.9919±0.0018
0.634417	1.0017±0.0020	0.689946	0.9920±0.0019	0.740428	0.9888±0.0019	0.790187	0.9928±0.0021
0.635859	0.9980±0.0020	0.690667	0.9898±0.0019	0.741150	0.9897±0.0019	0.790907	0.9921±0.0019
0.636580	1.0037±0.0020	0.691389	0.9893±0.0019	0.741871	0.9927±0.0019	0.791629	0.9892±0.0018
0.638023	0.9992±0.0020	0.692831	0.9913±0.0019	0.742592	0.9873±0.0019	0.792350	0.9903±0.0019
0.638744	0.9972±0.0019	0.693552	0.9959±0.0019	0.743313	0.9915±0.0018	0.793071	0.9907±0.0018
0.639465	1.0027±0.0020	0.694273	0.9900±0.0019	0.744034	0.9920±0.0018	0.793792	0.9925±0.0018
0.640907	0.9985±0.0021	0.694994	0.9912±0.0019	0.744755	0.9864±0.0018	0.794513	0.9918±0.0019
0.641628	1.0026±0.0020	0.696437	0.9929±0.0019	0.745476	0.9931±0.0018	0.795235	0.9912±0.0019
0.642350	0.9997±0.0019	0.697158	0.9838±0.0019	0.746198	0.9924±0.0019	0.795956	0.9923±0.0019
0.643071	1.0045±0.0020	0.697879	0.9926±0.0019	0.746919	0.9881±0.0019	0.796677	0.9919±0.0019
0.643792	1.0013±0.0020	0.698600	0.9906±0.0019	0.747640	0.9885±0.0018	0.797398	0.9921±0.0019
0.644513	1.0018±0.0020	0.699321	0.9886±0.0019	0.748361	0.9934±0.0019	0.798119	0.9904±0.0020
0.645234	0.9981±0.0020	0.700043	0.9916±0.0019	0.749082	0.9918±0.0019	0.799562	0.9933±0.0020
0.645955	1.0018±0.0020	0.700764	0.9899±0.0019	0.750524	0.9888±0.0018	0.800283	0.9931±0.0021
0.646677	0.9985±0.0019	0.701485	0.9885±0.0019	0.751246	0.9880±0.0018	0.801004	0.9937±0.0021
0.647398	0.9976±0.0020	0.702206	0.9883±0.0019	0.751967	0.9882±0.0019	0.801725	0.9993±0.0022
0.648119	1.0012±0.0020	0.702927	0.9901±0.0019	0.752688	0.9924±0.0019	0.802446	0.9911±0.0023
0.648840	1.0027±0.0020	0.703649	0.9928±0.0019	0.753409	0.9970±0.0019	0.803167	0.9934±0.0023
0.649561	1.0001±0.0020	0.704370	0.9926±0.0019	0.754130	0.9894±0.0019	0.803889	0.9934±0.0024
0.651004	0.9988±0.0019	0.705091	0.9910±0.0019	0.754851	0.9913±0.0018	0.804610	0.9969±0.0026
0.651725	0.9993±0.0019	0.705812	0.9895±0.0019	0.755573	0.9891±0.0018	0.805331	0.9954±0.0027
0.652446	0.9994±0.0019	0.706533	0.9984±0.0019	0.756294	0.9932±0.0019	0.806052	0.9996±0.0028
0.653167	0.9977±0.0019	0.707254	0.9907±0.0019	0.757015	0.9930±0.0019	0.806773	0.9988±0.0031
0.653889	0.9948±0.0020	0.707975	0.9928±0.0019	0.757736	0.9918±0.0019	0.807494	0.9926±0.0033
0.654610	0.9988±0.0020	0.708697	0.9859±0.0019	0.758457	0.9946±0.0022	0.808215	0.9928±0.0035
0.655331	0.9965±0.0020	0.709418	0.9852±0.0019	0.759178	0.9911±0.0019	0.808937	0.9956±0.0039
0.656052	0.9960±0.0020	0.710139	0.9888±0.0019	0.759899	0.9882±0.0019	0.809658	0.9973±0.0043
0.656774	0.9967±0.0019	0.711581	0.9907±0.0019	0.761342	0.9923±0.0018	0.810379	0.9974±0.0045
0.657494	0.9901±0.0019	0.712302	0.9917±0.0019	0.762063	0.9909±0.0018	0.811100	0.9992±0.0049
0.658216	0.9970±0.0020	0.713024	0.9890±0.0019	0.762784	0.9873±0.0018	0.811822	0.9967±0.0056
0.658937	0.9961±0.0022	0.714466	0.9886±0.0019	0.763505	0.9895±0.0018	0.812543	1.0004±0.0061
0.659658	1.0041±0.0024	0.715187	0.9909±0.0018	0.764226	0.9877±0.0018	0.813264	0.9993±0.0068
0.660379	0.9939±0.0029	0.715908	0.9902±0.0018	0.764948	0.9883±0.0018	0.813985	0.9987±0.0071
0.661100	0.9980±0.0031	0.716630	0.9878±0.0019	0.765669	0.9902±0.0018	0.814707	0.9935±0.0078
0.662543	0.9961±0.0020	0.717351	0.9890±0.0019	0.766390	0.9874±0.0018	0.815428	1.0070±0.0090
0.663264	0.9941±0.0019	0.718072	0.9850±0.0019	0.767111	0.9911±0.0018	0.816149	1.0019±0.0095
0.663985	0.9950±0.0019	0.718793	0.9889±0.0019	0.767832	0.9907±0.0018	0.816870	1.0001±0.0109
0.664706	0.9936±0.0020	0.719514	0.9894±0.0019	0.768553	0.9894±0.0018		

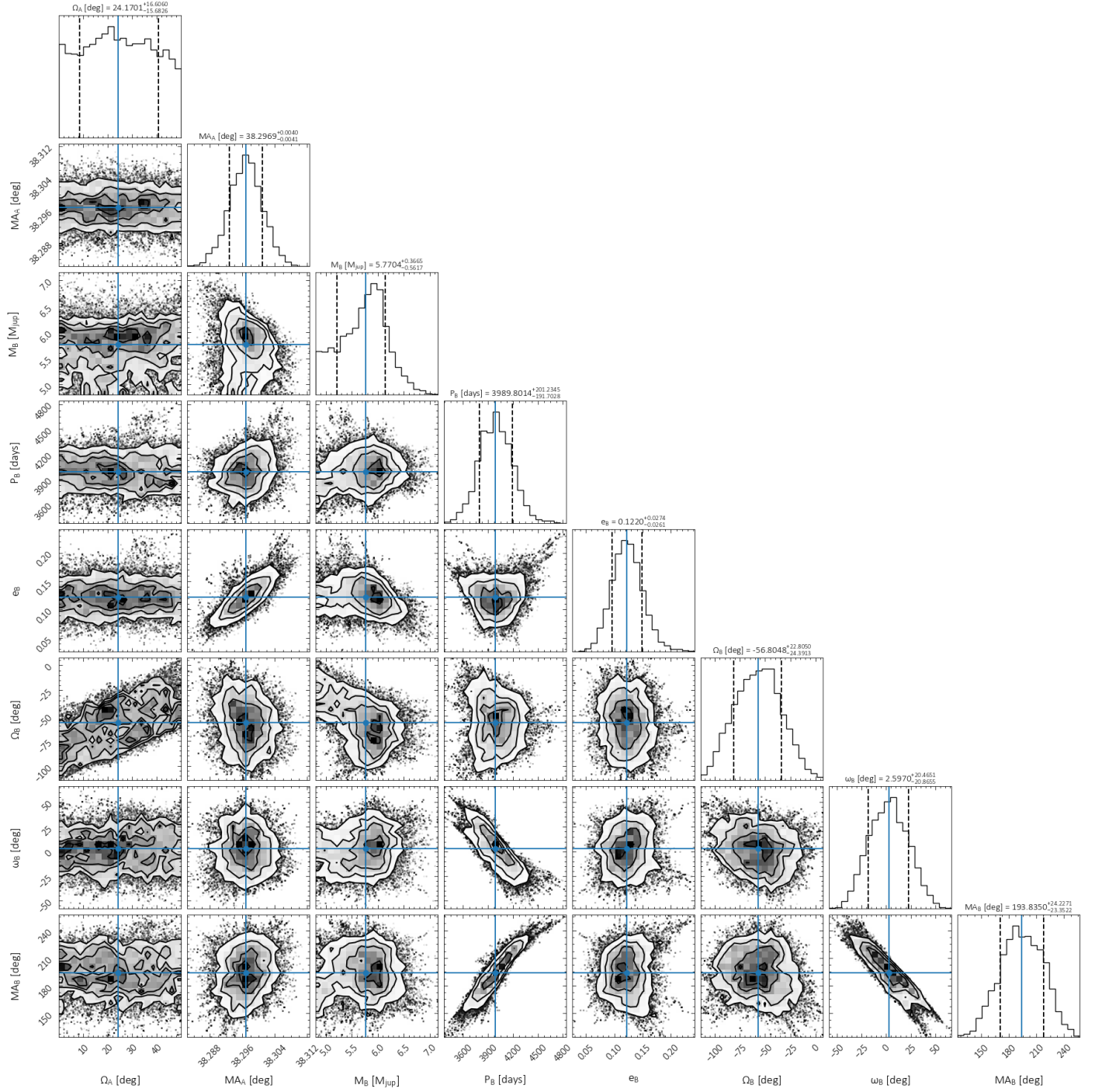


**Fig. A.2.** Corner plot for the a posteriori distribution of our free orbital parameters of TOI-4562 b and TOI-4562 c derived from our analysis. The values for the orbital parameters are listed in Table 2.



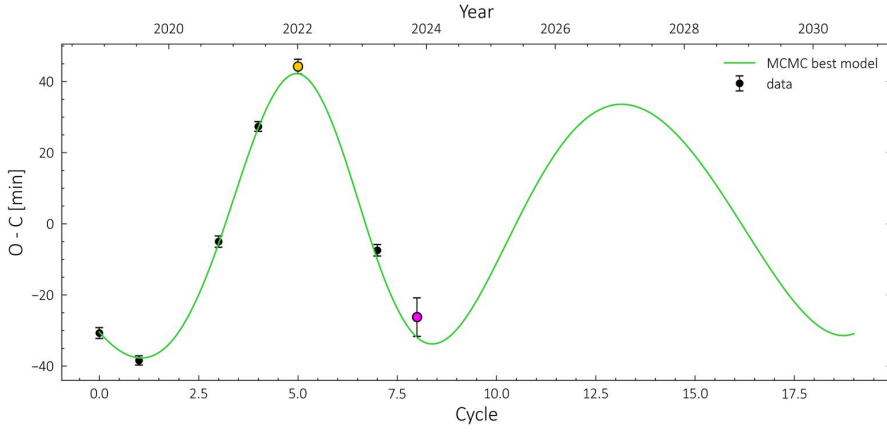


**Fig. A.3.**  $O - C$  diagram of the observed (circles with error bars) and modelled (solid green line) data for the already observed and future cycles. The calculated midtransits for cycles #10 to #15 are presented in Table A.2.

**Table A.2.** Midtransits for the next TOI-4562 b events

Cycle	Transit Mid-time BJD [days]	Transit Date [UT]	Visibility
10	2,460,707.95681	2025-02-01 UT 10:57:47	Oceania, Antarctica
11	2,460,933.07844	2025-09-14 UT 13:52:57	Oceania
12	2,461,158.19603	2026-04-27 UT 16:42:17	Oceania, Africa
13	2,461,383.30698	2026-12-08 UT 19:22:03	Africa, Antarctica
14	2,461,608.41116	2027-07-21 UT 21:52:04	Africa
15	2,461,833.50982	2028-03-03 UT 00:14:08	South America, Africa

**Notes.** Midtransits for the next five transits of TOI-4562 b according with the ephemeris and TTVs described in our work. Locations in the Southern Hemisphere where the transit would be observable from ground-based telescopes are also presented. Full or partial coverage will depend on the observatory coordinates.